Downlink Performance Analysis of Extremely Large-Scale MIMO-OFDM Systems for High-Speed Railway

Wenhui Yi [ID], Jiayi Zhang [ID], *Senior Member, IEEE*, Zhe Wang [ID], Huahua Xiao [ID], and Bo Ai [ID]

Abstract—The potential of extremely large-scale multiple-input multiple-output (XL-MIMO) systems to enhance the performance of high-speed railway (HSR) wireless networks is vast. In this correspondence, we examine the performance characteristics of the XL-MIMO-OFDM HSR system, focusing on uniform planar array (UPA) and uniform linear array (ULA) configurations. Considering the multipath spherical wave channel model, we develop a system model that accounts for the Doppler frequency offset (DFO) caused by train movement. Our analysis includes the performance of effective degrees of freedom (EDoF), deriving closed-form expressions for both UPA- and ULA-based systems. Additionally, we investigate the integration of XL-MIMO with orthogonal frequency-division multiplexing (OFDM), which enhances the signal-to-interference plus noise ratio (SINR) and spectral efficiency (SE) of individual base stations. Simulation results demonstrate the superior EDoF performance of UPA- and ULA-based XL-MIMO-OFDM systems. Moreover, the intercarrier interference resulting from train movement increases with speed, and the degradation in signal quality caused by this interference can be mitigated by configuring the XL-MIMO-OFDM system. Notably, the adoption of XL-MIMO technology with a near-field channel model significantly improves coverage reliability compared to traditional MIMO configurations using a far-field channel model.

Index Terms—XL-MIMO-OFDM, HSR networks, near-field, effective degrees of freedom, spectral efficiency.

I. INTRODUCTION

The recent endorsement by the Ministry of Industry and Information Technology of China regarding the frequency testing of the railway's next-generation mobile communication system (5G-R) marks a significant milestone, heralding a new phase in high-speed railway (HSR) infrastructure development [1], [2]. Compared to the global system of mobile communication for railways (GSM-R) and long-term evolution for railways (LTE-R) [3], the emerging generation of HSR communication networks is characterized by expansive bandwidth, ultra-low latency, and extensive connectivity capabilities. Furthermore, as an inherently closed railway network, heightened emphasis is placed on ensuring stringent security protocols and bolstering overall system reliability [4], [5], [6].

To satisfy various stringent demands for HSR communication, various promising technologies have been widely studied. In [7], the authors introduced the fundamental performance of 5G-R systems

Wenhui Yi, Jiayi Zhang, Zhe Wang, and Bo Ai are with the State Key Laboratory of Advanced Rail Autonomous Operation Beijing 100044, China, and also with the School of Electronics and Information Engineering, Beijing Jiaotong University, Beijing 100044, China (e-mail: wenhuiyi@bjtu.edu.cn; jiayizhang@bjtu.edu.cn; zhewang_77@bjtu.edu.cn; boai@bjtu.edu.cn).
Huahua Xiao is with the ZTE Corporation, State Key Laboratory of Mobile Network and Mobile Multimedia Technology, Shenzhen 518055, China (e-mail: xiao.huahua@zte.com.cn).
Digital Object Identifier 10.1109/TVT.2025.3547384

employing linear redundant coverage and analyzed inter-cell interference's impact on cell edge users' capacity based on a hybrid channel model. Moreover, the authors in [8] studied the coverage performance for cell-free (CF) massive multiple-input multiple-output (mMIMO) HSR communication systems. Considering the Doppler frequency offset (DFO) leads to inter-carrier interference (ICI) within the context of orthogonal frequency division multiplexing (OFDM) technology, the author in [9] analyzed the performance of CF mMIMO-OFDM systems in HSR communications. The present HSR systems rely on mMIMO technology or CF mMIMO technology. Nevertheless, the technology examined in the research mentioned above has minimal demands for widespread deployment of intelligent HSR in the future. Recent studies have increasingly highlighted the advantages of near-field communication technology compared with far-field communication technology in technical aspects like channel estimation, beamforming, and positioning. Consequently, the extremely large-scale multiple-input-multiple-output (XL-MIMO), offering extensive spatial flexibility and an expanded near-field communication range, demonstrates significant promise in the realm of future HSR [10].

As an evolution of MIMO, the fundamental principle of XL-MIMO entails the strategic placement of a multitude of antennas within a limited spatial domain, and there are mainly two different designs called uniform linear array (ULA) and uniform planar array (UPA) for XL-MIMO systems [11]. This strategic approach serves to augment the effective degrees of freedom (EDoF) [10], thereby enhancing the efficiency of data stream transmission. Furthermore, XL-MIMO technology and OFDM technology can be combined and applied in HSR communication to improve spectrum efficiency and robustness against frequency selective fading [9], [12]. In XL-MIMO-OFDM HSR scenarios, DFO can instigate ICI and significantly diminish the performance of systems. In assessing the efficacy of HSR systems, coverage reliability is a pivotal metric. This significance stems from the potential consequences of communication link degradation, which can significantly impact the safety and operational efficiency of railway networks [7].

In this correspondence, we study the downlink XL-MIMO-OFDM HSR communication system, focusing on the EDoF and spectral efficiency (SE) performance. Firstly, we develop the XL-MIMO-OFDM multi-user communication system model for HSR and the performance analysis framework over the near-field channel. Then, we derive closed-form expressions of EDoF for both UPA- and ULA-based HSR systems. Moreover, we present the expression of signal-to-interference plus noise ratio (SINR) and SE considering the ICI caused by DFO. Finally, numerical results reveal the EDoF performance of UPA- and ULA-based XL-MIMO systems. Notably, the interference caused by movement is directly related to the speed of motion. However, the resulting degradation in signal quality can be effectively mitigated by deploying large array antennas. Furthermore, compared to the far-field model, adopting the near-field model for performance analysis in this system yields greater accuracy and effectiveness.

II. SYSTEM MODEL

We consider the downlink UPA-based XL-MIMO-OFDM HSR communication system, shown in Fig. 1. One target BS is considered, which is located in the $x-y$ plane with its center at
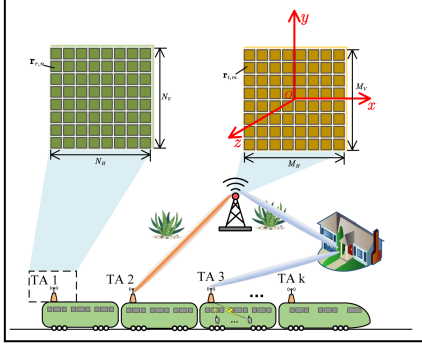
Fig. 1.   XL-MIMO-OFDM HSR communication systems.

TABLE I
SYSTEM MODEL PARAMETER TABLE

Definition	Symbol
The number of transmitter row antenna	M_H
The number of receiver row antenna	N_H
The number of transmitter column antenna	M_V
The number of receiver column antenna	N_V
Transmitter horizontal length	$L_{t,H}$
Receiver horizontal length	$L_{r,H}$
Transmitter vertical length	$L_{t,V}$
Receiver vertical length	$L_{r,V}$
Transmitter center position	$[0,0,0]^T$
Receiver center position	$[x_r, y_r, z_r]^T$
The m-th transmitting antenna horizontal index	$i(m) = \mathrm{mod}(m-1, M_H)$
The n-th receiving antenna horizontal index	$q(n) = \mathrm{mod}(n-1, N_H)$
The m-th transmitting antenna vertical index	$j(m) = \lfloor (m-1)/M_H \rfloor$
The n-th receiving antenna vertical index	$k(n) = \lfloor (n-1)/N_H \rfloor$

the origin. The BS is equipped with UPA-based XL-MIMO, consisting of $M = M_H \times M_V$ discrete point antennas. The horizontal spacing between transmitter antennas is $\Delta_{t,H} = L_{t,H}/M_H$, and the vertical spacing between transmitter antennas is $\Delta_{t,V} = L_{t,V}/M_V$. The position of the m-th antenna on the target transmitter is $\mathbf{r}_{t,m} = [-\frac{L_{t,H}}{2} + i(m)\Delta_{t,H}, -\frac{L_{t,V}}{2} + j(m)\Delta_{t,V}, 0]^T$ [13], [14], with $m \in \{1, \ldots, M\}$. Meanwhile, we consider that a mobile train, which is equipped with U carriages, moves along the y-axis with a velocity denoted as v, and the vector of velocity is denoted as $\mathbf{v} = [v, 0, 0]^T$. Each carriage is equipped with a UPA-based XL-MIMO system with $N = N_H \times N_V$ discrete point antennas, which serves as a relay station for communication with the BS. The horizontal spacing between receiver antennas is $\Delta_{r,H} = L_{r,H}/N_H$, and the vertical spacing between receiver antennas is $\Delta_{r,V} = L_{r,V}/N_V$. With the position of the center of the u-th receiver being denoted as $[x_r^u, y_r^u, z_r^u]^T$, the position of the n-th antenna on the u-th receiver is $\mathbf{r}_{r,n}^u = [x_r^u - \frac{L_{r,H}}{2} + q(n)\Delta_{r,H}, y_r^u - \frac{L_{r,V}}{2} + k(n)\Delta_{r,V}, z_r^u]^T$ with $n \in \{1, \ldots, N\}$, and the distance between the centers of the target transmitter and the receiver is denoted as $d = \sqrt{x_r^{u2} + y_r^{u2} + z_r^{u2}}$. Considering the XL-MIMO-OFDM channel in the HSR communication scenario as shown in Fig. 2, there exists ICI between adjacent subcarriers. In specific applications, cyclic prefix (CP) OFDM and zero padding (ZP) OFDM can reduce ICI by adding a guard interval (GI) larger than the channel length. However, this correspondence primarily emphasizes investigating ICI resulting from the DFO, so we do not consider the configuration of GI. The bandwidth is B, the duration of an OFDM symbol is T_s, and
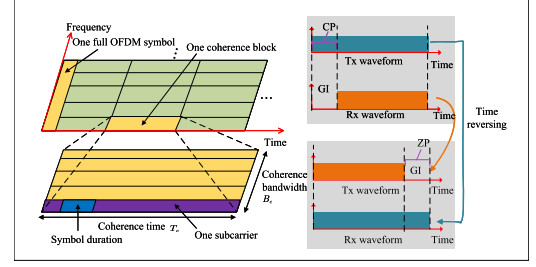

Fig. 2.   OFDM channel with intercarrier interference.

the number of the total subcarriers is L_{total}. High-speed movements in HSR scenarios result in large DFOs. The ICI due to the DFO effect gradually decays as the number of intervening subcarriers increases. It is found that the variance of the ICI coefficients of the adjacent subcarriers is less than 10^{-2} from the fourth. Therefore, we can use a complete OFDM transmission in a real systems, but study only one of the blocks including $L \geq 8$ subcarriers for an approximate analysis with a small error [9].

The HSR channel consisting of the (line-of-sight) LoS and (Non-Line-of-Sight) NLOS components is considered. We define the downlink channel vector between the BS and the u-th train relays as $\mathbf{H}_u = \bar{\mathbf{H}}_u + \check{\mathbf{H}}_u \in \mathbb{C}^{N \times M}$, where $\bar{\mathbf{H}}_u$ and $\check{\mathbf{H}}_u$ are the LoS and NLoS components, respectively. For the LoS component $\bar{\mathbf{H}}_u$, we apply the non-uniform spherical wave propagation model introduced in [11]. We define the (n, m)-th element of $\bar{\mathbf{H}}_u$ is $[\bar{\mathbf{H}}_u]_{nm} = \sqrt{\beta_u^{los}} \frac{d}{d_{mn}} e^{-j\frac{2\pi}{\lambda}(d_{mn}-d)}$, where $d_{mn} = |\mathbf{r}_{r,n}^u - \mathbf{r}_{t,m}|$ is the distance between the m-th antenna of the BS and the n-th antenna of the u-th receiver, λ is the wavelength, and $\beta_u^{los} = \sqrt{\frac{K}{1+K}}\beta_u$ is the large-scale fading coefficient for the LoS component between BS and receiver u, where K is Rician factor and β_u is the total large-scale fading coefficient.

For the NLoS component $\check{\mathbf{H}}_u$, we model it with the Fourier plane-wave representation method. We denote that $a_{r,n}^u(k_x, k_y, \mathbf{r}_{r,n}^u) = e^{j[k_x r_{rn,x}^u + k_y r_{rn,y}^u + \gamma(k_x,k_y)r_{rn,z}^u]}$ and $a_{s,m}(\kappa_x, \kappa_y, \mathbf{r}_{t,m}) = e^{-j[\kappa_x r_{tm,x} + \kappa_y r_{tm,y} + \gamma(\kappa_x,\kappa_y)r_{tm,z}]}$ are the receiving response and the transmitting response, respectively, with $\mathbf{r}_{t,m} = [r_{tm,x}, r_{tm,y}, r_{tm,z}]^T$ and $\mathbf{r}_{r,n}^u = [r_{rn,x}^u, r_{rn,y}^u, r_{rn,z}^u]^T$. Moreover, the receiving wave vector is $\mathbf{k} = [k_x, k_y, k_z]^T$, the transmitting wave vector is $\boldsymbol{\kappa} = [\kappa_x, \kappa_y, \kappa_z]^T$, $\gamma(k_x, k_y) = (k^2 - k_x^2 - k_y^2)^{1/2}$, and $\mathcal{D} = \{(k_x, k_y) \in \mathbb{R}^2 | k_x^2 + k_y^2 \leq \kappa^2\}$ denotes the integration region with $\kappa = 2\pi/\lambda$ being the wavenumber. Considering the isotropic scattering environment, the channel of u-th receiver can be expressed as [11]

$$\check{\mathbf{H}}_u \approx \sqrt{MN} \sum_{(\ell_x, \ell_y) \in \mathcal{E}_r} \sum_{(m_x, m_y) \in \mathcal{E}_s} H_{a,u}(\ell_x, \ell_y, m_x, m_y)$$
$$\mathbf{a}_{r,u}(\ell_x, \ell_y)\mathbf{a}_s^H(m_x, m_y), \quad (1)$$

where the n-th element of $\mathbf{a}_{r,u}(\ell_x, \ell_y)$ is $[\mathbf{a}_{r,u}(\ell_x, \ell_y)]_n = \frac{1}{\sqrt{N}}a_{r,n}^u(\frac{2\pi\ell_x}{L_{r,H}}, \frac{2\pi\ell_y}{L_{r,V}}, \mathbf{r}_{r,n}^u)$, the m-th element of $\mathbf{a}_s(m_x, m_y)$ is $[\mathbf{a}_s(m_x, m_y)]_m = \frac{1}{\sqrt{M}}a_{s,m}(\frac{2\pi m_x}{L_{t,H}}, \frac{2\pi m_y}{L_{t,V}}, \mathbf{r}_{t,m})$, $\mathcal{E}_r = \{(\ell_x, \ell_y) \in \mathbb{Z}^2 : (\ell_x\lambda/L_{r,H})^2 + (\ell_y\lambda/L_{r,V})^2 \leq 1\}$ is the lattice ellipse at the receiver, and $\mathcal{E}_t = \{(m_x, m_y) \in \mathbb{Z}^2 : (m_x\lambda/L_{t,H})^2 + (m_y\lambda/L_{t,V})^2 \leq 1\}$ is the lattice ellipse at the transmitter. Moreover, we have $H_{a,u}(\ell_x, \ell_y, m_x, m_y) \sim \mathcal{CN}(0, \beta_u^{nlos}\bar{\sigma}_u(\ell_x, \ell_y, m_x, m_y))$, where $\beta_u^{nlos} = \sqrt{\frac{1}{1+K}}\beta_u$ is the large-scale fading coefficient for NLoS

component between the BS and receiver u, and $\bar{\sigma}_u(\ell_x, \ell_y, m_x, m_y)$ is the normalized variance at the sampling point (ℓ_x, ℓ_y) and (m_x, m_y).

We assume that different signals are set at different subcarriers. Then, with $l \in \{1, \ldots, L\}$ and $s \in \{1, \ldots, L\}$ denoting the subcarrier index, the total received signal from BS to the u-th receiver can be expressed in the frequency domain as

$$\mathbf{y}_u[s] = \sqrt{p} \sum_{l=1}^{L} \sum_{i=1}^{U} \mathbf{H}_u[l-s] \mathbf{w}_i[l] \mathbf{x}_i[l] + \mathbf{n}[s], \quad (2)$$

where p is the downlink transmit power, the channel matrix affected by ICI is $\mathbf{H}_u[l-s] = \mathbf{I}_{los}^u[l-s] \odot \bar{\mathbf{H}}_u + I_{nlos}[l-s]\check{\mathbf{H}}_u \in \mathbb{C}^{N \times M}$, where $\mathbf{I}_{los}^u[l-s] \in \mathbb{R}^{N \times M}$ and $I_{nlos}[l-s]$ are the ICI coefficient for LoS component and NLoS component, respectively. Moreover, $\mathbf{y}_u[s] \in \mathbb{C}^{N \times 1}$ is the received signals for u-th receiver, $\mathbf{w}_i[l] \in \mathbb{C}^{M \times N}$ is the precoding matrix for i-th receiver, with $i \in \{1, \ldots, U\}$, $\mathbf{x}_i[l] \in \mathbb{C}^{N \times 1}$ is the transmitted signal for i-th receiver to l-th subcarrier with $\mathbb{E}\{|\mathbf{x}_i[l]|^2\} = 1$, $\mathbf{n}[s] \in \mathbb{C}^{N \times 1}$ is the additive noise with independent $\mathcal{N}_{\mathbb{C}}(0, \sigma^2)$ elements, and σ^2 being the noise power, which can be calculated by the relationship between temperature, bandwidth, and noise coefficient [8].

Lemma 1: The ICI interference coefficients for the (n, m)-th LOS component and the NLOS component are expressed as

$$[\mathbf{I}_{los}^u[l-s]]_{nm} = \frac{\sin(\pi(l-s+f_{nor,n,m}))}{L \sin\left(\frac{\pi}{L}(l-s+f_{nor,n,m})\right)}$$

$$\times \exp\left(j\pi(1 - \frac{1}{L})(l-s+f_{nor})\right),$$

$$I_{nlos}[l-s] = \begin{cases} 1, l = s, \\ \frac{(-1)^{l-s}\omega}{\sqrt{2(l-s)}}, l \neq s, \end{cases} \quad (3)$$

where $f = f_c + \frac{2l-L-1}{2T_s}$ is the carrier frequency of the l-th subcarrier, f_c is the center carrier frequency, c is the speed of light, $f_{nor,n,m} = \omega\varphi(n,m) = \frac{-fvT_s}{c}\varphi(n,m)$ is the normalized DFO between the m-th transmitter antenna and the n-th receiver antenna with $\varphi(n,m) = \frac{(\mathbf{r}_{r,n}-\mathbf{r}_{t,m})\cdot\mathbf{v}}{|\mathbf{r}_{r,n}-\mathbf{r}_{t,m}|v}$ being the cosine of the angle between the signal propagation direction and the train's operational direction.

Proof: The XL-MIMO equipped with M transmitting antennas and N receiving antennas has total $M \times N$ channels. Due to the size of UPA, the DFO of each channel may not necessarily be equal, and we use one of the channels as an example to prove this.

Let donate $x[l]$ as the discrete baseband symbols on each subcarrier, and process the received signal after DFT is expressed as $y[s] = \sum_{m=0}^{L-1} x[l] \frac{1}{L} \sum_{n=0}^{L-1} \exp(j2\pi \frac{n}{L}(l-s+f_{nor})) + w[s]$ [9], [18], where $s = 1, \ldots L-1$, f_{nor} is the normalized DFO and $w[s]$ is the DFT of the noise. Then we simplify the expression of the subcarrier interference coefficient as

$$\frac{1}{L} \sum_{n=0}^{L-1} \exp\left(j2\pi \frac{n}{L}(l-s+f_{nor})\right)$$

$$= \frac{1}{L} \sum_{n=0}^{L-1} e^{(j2\pi \frac{1}{L}(l-s+f_{nor}))n} \overset{(b)}{\approx} \frac{1}{L} \frac{1 - e^{(j2\pi \frac{1}{L}(l-s+f_{nor}))L}}{1 - e^{(j2\pi \frac{1}{L}(l-s+f_{nor}))}}$$

$$= \frac{1}{L} \frac{\left(1 - e^{j2\pi(l-s+f_{nor})}\right)/e^{j\pi(l-s+f_{nor})}}{\left(1 - e^{j2\pi \frac{1}{L}(l-s+f_{nor})}\right)/e^{j\pi \frac{1}{L}(l-s+f_{nor})}} \times \frac{e^{j\pi(l-s+f_{nor})}}{e^{j\pi \frac{1}{L}(l-s+f_{nor})}}$$

$$= \frac{\left(e^{j\pi(l-s+f_{nor})} - e^{-j\pi(l-s+f_{nor})}\right)}{L\left(e^{j\pi \frac{1}{L}(l-s+f_{nor})} - e^{-j\pi \frac{1}{L}(l-s+f_{nor})}\right)} e^{(j\pi(1-\frac{1}{L})(l-s+f_{nor}))}$$

$$\overset{(c)}{\approx} \frac{\sin(\pi(l-s+f_{nor}))}{L \sin\left(\frac{\pi}{L}(l-s+f_{nor})\right)} \exp\left(j\pi(1 - \frac{1}{L})(l-s+f_{nor})\right), \quad (4)$$

where the approximation (b) is $\sum_{n=0}^{L-1} a^n = \frac{1-a^L}{1-a}$, and the approximation (c) is $\sin(x) = \frac{e^{jx}-e^{-jx}}{2j}$. For the LoS path with fixed $f_{nor,n,m}$, we obtain the ICI coefficients of LoS component. For a sufficient number of NLOS paths with independent and identically distributed AOAs and amplitudes, we follow the same steps as above and obtain the statistical ICI coefficients of the NLOS paths as the final interference coefficient result.

III. EDoF ANALYSIS

In this section, we analyze the EDoF performance of the transmitter BS_0 and the rapidly moving train leveraging the scalar Green's function channels. Moreover, we compute EDoF expressions for the UPA- and ULA-based XL-MIMO-OFDM HSR systems in the closed form. For XL-MIMO wireless communications with discrete antennas, the channel capacity can be computed as the sum capacity of multiple SISO channels, and EDoF represents the number of equivalent independent single-input-single-output (SISO) channels and takes into account channel characteristics and interference. So EDoF can be used as an important metric to measure the performance of the XL-MIMO-OFDM HSR system [11].

A. EDoF Analysis for UPA-Based XL-MIMO

In this subsection, we analyze the UPA-based XL-MIMO-OFDM HSR system, where the target transmitter and one receiver are equipped with UPA-based XL-MIMO. The channel correlation matrix for u-th receiver is represented by $\mathbf{R}_u = \mathbb{E}\{\mathbf{H}_u^*\mathbf{H}_u\} \in \mathbb{C}^{M \times M}$. Since the LoS component and NLoS component are independent of each other, the EDOF can be calculated by [16]

$$\varepsilon \approx \frac{(\mathrm{tr}(\mathbf{R}))^2}{\mathrm{tr}(\mathbf{R}^2)} = \frac{(\mathrm{tr}(\bar{\mathbf{H}}_u^*\bar{\mathbf{H}}_u) + \mathrm{tr}(\mathbb{E}\{\check{\mathbf{H}}_u^*\check{\mathbf{H}}_u\}))^2}{\mathrm{tr}((\bar{\mathbf{H}}_u^*\bar{\mathbf{H}}_u)^2) + \mathrm{tr}(\mathbb{E}\{\check{\mathbf{H}}_u^*\check{\mathbf{H}}_u\})^2)}. \quad (5)$$

Based on (2), we consider the EDoF of the desired signal for u-th receiver to express the maximum of transmitting data streams shown as

$$\varepsilon_{UPA}^u = \max\{\varepsilon^u[s]\} \approx \frac{(\mathrm{tr}(\mathbb{E}\{\mathbf{H}_u[0]^*\mathbf{H}_u[0]\}))^2}{\mathrm{tr}((\mathbb{E}\{\mathbf{H}_u[0]^*\mathbf{H}_u[0]\})^2)}, \quad (6)$$

where $s = 1, 2, \ldots, L$ and $l = s$.

Remark 1: By completely calculating the EDOF expressed as (5) according to the single carrier, the EDOF can be determined for any channel matrix corresponding to l and s. In conjunction with the EDOF definition, we only calculate the expected channel matrix without considering the interference channel gain, i.e. $l = s$. Furthermore, the maximum value of the transmitted data stream corresponding to the multi-carrier channel is utilized as the EDOF value under the multi-carrier channel, representing the upper limit of the system's transmission efficiency.

Lemma 2: EDoF of the UPA-based XL-MIMO-OFDM HSR system can be computed in the closed form as (7), shown at the bottom of the next page, where $f_d(m_1, m_2) = \frac{f_{nor,n,m_1}+f_{nor,n,m_2}}{2}$ denotes the average DFO of the m_1-th and m_2-th transmitting antennas, $d_x(n,m) = |x_r - \frac{L_{r,H}}{2} + q(n)\Delta_{r,H} + \frac{L_{t,H}}{2} - i(m)\Delta_{t,H}|$ and $d_y(n,m) = |y_r - \frac{L_{r,V}}{2} + k(n)\Delta_{r,V} + \frac{L_{t,V}}{2} - j(m)\Delta_{t,V}|$ are the horizontal distance and the vertical distance between the n-th antenna of the receiver and m-th antenna of the transmitter, respectively. And $\mathbf{R}_{nlos}^u \in \mathbb{C}^{M \times M}$ is the connection matrix for NLoS paths, and $[\mathbf{R}_{nlos}^u]_{ab}$ is the (a, b)-th element of $\mathbf{R}_{nlos}^u$.

Proof: For the UPA-based system, the (m_1, m_2)-th element of the connection matrix $\mathbf{R}_{los}^u = (\mathbf{I}_{los}^u[l-s] \odot \bar{\mathbf{h}}_u)^* (\mathbf{I}_{los}^u[l-s] \odot \bar{\mathbf{h}}_u) \in \mathbb{C}^{M \times M}$ for LoS path of u-th receiver with $m_1, m_2 \in \{1, \ldots, M\}$ is expressed as

$$
[\mathbf{R}_{los}^u]_{m_1 m_2} = \sum_{n=1}^{N} \left[\mathbf{I}_{los}^u[0] \odot \bar{\mathbf{H}}_u[0] \right]_{nm_1}^* \left[\mathbf{I}_{los}^u[0] \odot \bar{\mathbf{H}}_u[0] \right]_{nm_2}
$$

$$
= \sum_{n=1}^{N} \frac{\beta_u^{los} d^2}{d_{nm_1} d_{nm_2} e^{j\frac{2\pi}{\lambda}(d_{nm_2} - d_{nm_1})}} \frac{\sin^2(\pi f_d(m_1, m_2))}{L^2 \sin^2\left(\frac{\pi}{L} f_d(m_1, m_2)\right)}
$$

$$
\overset{a}{\approx} \sum_{n=1}^{N} \frac{\beta_u^{los}}{e^{j\frac{2\pi}{\lambda}(d_{m_2 n} - d_{m_1 n})}} \frac{\sin^2(\pi f_d(m_1, m_2))}{L^2 \sin^2\left(\frac{\pi}{L} f_d(m_1, m_2)\right)},
\tag{8}
$$

where the approximation (a) is $d_{m_1 n} d_{m_2 n} \approx d^2$.

Besides, $\mathbf{R}_{nlos}^u = \mathbb{E}\{\tilde{\mathbf{H}}^* \tilde{\mathbf{H}}\}$. Then, We can prove (7) by the following equation

$$
\varepsilon_{UPA}^u = \frac{\left| \sum_{m=1}^{M} (K[\mathbf{R}_{los}^u]_{mm} + [\mathbf{R}_{nlos}^u]_{mm}) \right|^2}{\sum_{m_1=1}^{M} \sum_{m_2=1}^{M} \left(\left| K[\mathbf{R}_{los}^u]_{m_1 m_2} \right|^2 + \left| [\mathbf{R}_{nlos}^u]_{m_1 m_2} \right|^2 \right)}.
\tag{9}
$$

Remark 2: The EDoF performance for XL-MIMO-OFDM HSR communication systems depends on the array size of UPA, the number of antennas, and the distance. Note that when $d \to \infty$, we can obtain $\varepsilon = 1$. This means the XL-MIMO system in free space can only transmit one data stream in the far-field [17].

B. EDoF Analysis for ULA-Based XL-MIMO

In this subsection, we study the ULA-based XL-MIMO-OFDM HSR system. Considering $N_H = M_H = 1$, we can obtain the ULA-based XL-MIMO-OFDM HSR system model with $L_{t,H}$ and $L_{r,H}$ ignored. The position of the m-th antenna on the transmitter is $\mathbf{r}_{t,m} = [0, -\frac{L_{t,V}}{2} + (m-1)\Delta_{t,V}, 0]^T$. The position of the n-th antenna on the receiver is $\mathbf{r}_{r,n} = [x_r, y_r - \frac{L_{r,V}}{2} + (n-1)\Delta_{r,V}, z_r]^T$. Based on the channel as shown in (4) and the EDoF expressed in (6), we can compute the closed-form expression of the EDoF for the ULA-based XL-MIMO-OFDM HSR system as follows.

Lemma 3: The EDoF of the ULA-based XL-MIMO-OFDM HSR system has the following expression as (10), shown at the bottom of this page, where $d_y(n, m) = |y_r - \frac{L_r}{2} + n\Delta_r - \Delta_r + \frac{L_t}{2} - m\Delta_t + \Delta_t|$ is the vertical distance between the n-th antenna of the receiver and m-th antenna of the transmitter.

Proof: Following the same steps in the proof of Lemma 2, we can prove Lemma 3.

Remark 3: The EDoF performance for the ULA-based system is similar to that of the UPA-based system. Additionally, both horizontal and vertical dimensions are considered in the UPA-based antenna

deployment, which significantly influences EDoF, presenting a higher level of complexity compared to the ULA-based XL-MIMO-OFDM system [11].

IV. COVERAGE ANALYSIS

Considering a downlink UPA-based XL-MIMO-OFDM HSR system as shown in Fig. 1, there are a large number of transmit and receive antennas improving the transmission rate, enhancing spectral efficiency (SE), and increasing spatial multiplexing gain. The spatial multiplexing gain, representing the maximum number of independent data streams supported by the channel, can be computed using the formula $G = \min(M, N, rank(\mathbf{H}))$. Furthermore, the error performance of XL-MIMO-OFDM systems can be evaluated using metrics such as the bit error rate, symbol error rate, SINR, and block error rate. In this section, we evaluate the system coverage reliability by analyzing the SINR and SE.

The received signal can be provided in the frequency domain in (2). Ensuring the stable coverage of railway communication networks is a crucial challenge in railway communication. To assess system coverage performance, metrics such as SINR, spectral efficiency (SE) [8], coverage probability and interruption probability [7] are commonly employed. In this scenario, we analyze SINR and SE to enable a comprehensive study of coverage performance[1].

Based on (2), the received signal of u-th receiver can be also expressed as

$$
\mathbf{y}_u[s] = \sqrt{p} \mathbf{H}_u[0] \mathbf{w}_u[s] \mathbf{x}_u[s] + \sqrt{p} \sum_{i \neq k}^{U} \mathbf{H}_u[0] \mathbf{w}_i[s] \mathbf{x}_i[s]
$$

$$
+ \sqrt{p} \sum_{l \neq s}^{L} \sum_{i=1}^{U} \mathbf{H}_u[l-s] \mathbf{w}_i[l] \mathbf{x}_i[l] + \mathbf{n}[s].
\tag{11}
$$

Based on the reciprocity of the uplink and downlink channels, we can write the precoding matrix to the u-th receiver using maximum ratio transmission (MRT), and minimum meansquare error (MMSE) precoding schemes:

$$
\mathbf{w}_u^{MMSE}[s] = \left(\sum_{l=1}^{L} \sum_{i=1}^{U} p \mathbf{H}_i^*[l-s] \mathbf{H}_i[l-s] + \sigma^2 \mathbf{I}_M \right)^{-1} \sqrt{p} \mathbf{H}_u^*[0],
$$

$$
\mathbf{w}_u^{MR}[s] = \sqrt{p} \mathbf{H}_u^*[0].
\tag{12}
$$

---

[1]It is necessary to study the technique of Doppler estimation and compensation for downlink channel in this scenario. There are methods effectively mitigating the effects of Doppler shifts, such as adaptive modulation and coding, dynamic frequency offset tracking, and optimized spectrum resource allocation. Due to the complexity and the space limitations of this correspondence, we will focus on these aspects in future research.

$$
\varepsilon_{UPA}^u = \frac{\left(\sum_{m=1}^{M} \left(K \sum_{n=1}^{N} \frac{\beta_u^{los} \sin^2(\pi f_d(m,m))}{L^2 \sin^2(\frac{\pi}{L} f_d(m,m))} + [\mathbf{R}_{nlos}^u]_{mm} \right) \right)^2}{\sum_{m_1=1}^{M} \sum_{m_2=1}^{M} \left(\left| \sum_{n=1}^{N} \frac{K \beta_u^{los} \sin^2(\pi f_d(m_1, m_2))}{L^2 \sin^2(\frac{\pi}{L} f_d(m_1, m_2)) e^{\frac{2\pi}{\lambda}(\sqrt{d_x(n,m_2)^2 + d_y(n,m_2)^2 + z_r^2} - \sqrt{d_x(n, m_1^2 + d_y(n,m_1)^2 + z_r^2)}}} \right|^2 + \left| [\mathbf{R}_{nlos}^u]_{m_1 m_2} \right|^2 \right)}.
\tag{7}
$$

$$
\varepsilon_{ULA}^u = \frac{\left(\sum_{m=1}^{M} \left(K \sum_{n=1}^{N} \frac{\beta_u^{los} \sin^2(\pi f_d(m,m))}{L^2 \sin^2(\frac{\pi}{L} f_d(m,m))} + [\mathbf{R}_{nlos}^u]_{mm} \right) \right)^2}{\sum_{m_1=1}^{M} \sum_{m_2=1}^{M} \left(\left| \sum_{n=1}^{N} \frac{K \beta_u^{los} \sin^2(\pi f_d(m_1, m_2))}{L^2 \sin^2(\frac{\pi}{L} f_d(m_1, m_2)) e^{\frac{2\pi}{\lambda}(\sqrt{x_r^2 + z_r^2 + d_y(n,m_2)^2} - \sqrt{x_r^2 + z_r^2 + d_y(n,m_1)^2})}} \right|^2 + \left| [\mathbf{R}_{nlos}^u]_{m_1 m_2} \right|^2 \right)}.
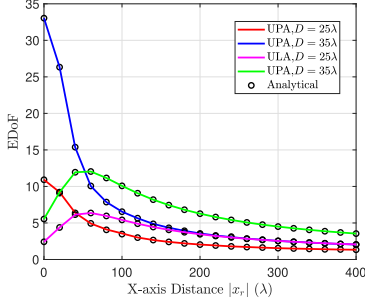\tag{10}
$$

Fig. 3. EDoF performance for XL-MIMO-OFDM HSR system against different values of $|x_r|$ with 15×15 antennas on UPA and 225 antennas on ULA.

Fig. 4. EDoF performance for XL-MIMO-OFDM HSR system against different numbers of antennas for both transmitter and receiver with $y_r = 20\lambda$.

After normalizing the above precoding matrix, it can be used for downlink transmission. By denoting $\mathbf{B}_{il}[l-s] = \sqrt{p}\mathbf{H}_u[l-s]\mathbf{w}_i[l] \in \mathbb{C}^{N \times N}(i = 1, 2, \ldots, U)$, we can obtain the interference matrix $\Xi[s] = \sum_{i=1}^{U}\sum_{l=1}^{L}\mathbf{B}_{il}[l-s]\mathbf{B}_{il}[l-s]^* - \mathbf{B}_{us}[0]\mathbf{B}_{us}[0]^* + \sigma^2\mathbf{I}_N$ and the expressions for SINR and SE

$$\text{SINR}_u[s] = \frac{\|\mathbf{B}_{us}[0]\|_F^2}{\|\Xi[s]\|_F},$$

$$\text{SE}_u[s] = \mathbb{E}\left\{\log_2\left|\mathbf{I}_N + \mathbf{B}_{us}[0]^H \Xi[s]^{-1} \mathbf{B}_{us}[0]\right|\right\}. \quad (13)$$

We use $\text{SINR}_u = \mathbb{E}\{\text{SINR}_u[s]\}$ and $\text{SE} = \sum_{u=1}^{U}\sum_{s=1}^{L}\text{SE}_u[s]/U$ to evaluate coverage performance. Then, we assume that the coverage probability represents the probability that SINR and SE are larger than the interrupt thresholds α_{th} and γ_{th}, respectively. Therefore, the coverage probability can be expressed as $\mathbb{P}_{cov} = \mathbb{P}\{\text{SINR}_u > \gamma_{th}, \text{SE}_u > \alpha_{th}\}$[7], [20]. When the antenna spacing is fixed, the array size will also increase with the number of antennas in XL-MIMO. The large-size array cannot directly reduce the value of DFO, but it can reduce the path loss of part of the received signal by decreasing the minimum communication distance between the transmitting antenna and the receiving antenna, thereby increasing the energy upper limit of the received signal and improving the system coverage performance.

V. NUMERICAL RESULTS

In this section, we present simulation results to validate our theoretical analysis for the EDoF of the HSR XL-MIMO-OFDM system and provide useful insights into the 5G-R deployment strategy based on the numerical results of one single BS coverage reliability. We consider that the number of antennas and the array designs of the transmitter and the receiver are equal. Besides, we define that the communication bandwidth $B = 20$ MHz, carrier frequency $f_c = 2.1$ GHz, a block subcarrier number $L = 8$, downlink transmit power $p = 200$ mW, sample duration $T_s = 67$ us, noise figure $N_F = 9$ dB, Rician factor $K = 30$ dB, wavelength $\lambda = \frac{c}{f_c}$, and distance between BS tower and rail $z_r = 2$ m [9]. In Fig. 3, we provide further validation of the EDoF closed-form results in **Lemma 2** and **Lemma 3** when one receiver runs through the target BS. We consider $v = 350$ km/h and the array aperture denoted as D, which is the side length for the ULA-based system and the length of the diagonal for the square UPA-based system, to represent the array size. The relative height between the BS and the train relay $|x_r| = 6$ m. As observed, the EDoF closed-form results, represented by "$\circ$", closely align with the simulation results depicted by the curves, confirming the accuracy of our derived EDoF closed-form expression over different values of the array aperture. Moreover, with the increase of the horizontal distance between the transmitter and the
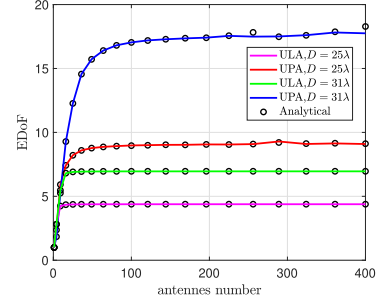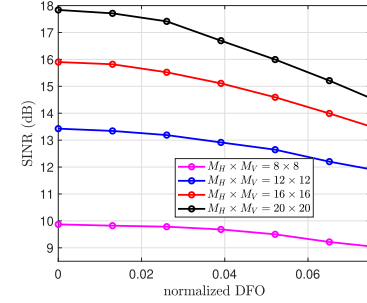

Fig. 5. SINR for XL-MIMO-OFDM HSR system against different values of the normalized DFO over different numbers of antennas equipped on the system.

receiver, the EDoF of the ULA-based system increases first and then decreases continuously. And it can be found that the UPA-based system demonstrates an enhancement mitigating signal quality degradation induced by trains traversing BS towers. This is because the UPA architecture enhances the spatial DoF in the horizontal direction, thereby increasing the spatial EDoF as receivers moving in the horizontal direction approach the BS.

In Fig. 4, we provide further validation of the EDoF closed-form versus different numbers of antennas equipped on the ULA- and square UPA-based single-user XL-MIMO system. We consider $v = 350$ km/h, and both transmitter and receiver install the same antenna array. The relative height between the BS and the train relay $|z_r| = 6$ m. It is found that the EDoF closed-form results, represented by "$\circ$", closely align with the simulation results depicted by the curves. Moreover, with the increase of the number of antennas, the EDoF of XL-MIMO continues to increase until it converges to a limit. According to [16], the limit is the EDOF value of continuous aperture XL-MIMO and the maximum number of effective data streams that can be transmitted by discrete aperture XL-MIMO.

Fig. 5 shows the SINR versus the normalized DFO between the centers of the transmitter and receiver of the train at different antenna numbers in single-user scenario. We assume that the train and the BS are deployed with the same UPA-based XL-MIMO with an antenna spacing of $\lambda/2 \times \lambda/2$. The relative height between the centers of the transmitting system and the receiving system $|z_r| = 10$ m. Due to the Doppler frequency shift caused by train movement, subcarrier interference occurs during signal transmission. With the increase of the train normalized DFO, the interference increases continuously, resulting in a descending SINR for trains to receive signals at the same position. It can be found that increasing the number of antennas can increase the SINR value, thereby improving the signal quality degradation caused by DFO, e.g. 7 dB SINR increase for $M_H \times M_V =$
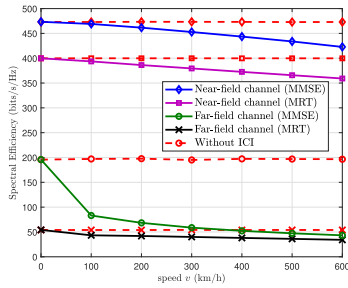
Fig. 6. SE versus the speed of the train with far-field and near-field channel model. We set $M_H = N_H$, $M_V = N_V$, the number of receiver $U = 4$, the position of the first receiver is $[0, -6\,m, 2\,m]^T$ and the user interval is $25\,m$.

20×20 compared with $M_H \times M_V = 8 \times 8$, for $y_r = -1000\,\text{m}$ and normalized DFO$= 0.04$ with $v = 300\,\text{km/h}$.

Fig. 6 shows that SE versus the speed of the train with far-field channel [10] and near-field channel for the square UPA-based XL-MIMO-OFDM HSR system. The near-field and far-field regions are typically bounded by the Rayleigh distance [11], which increases with antenna array size and frequency. In this study, we apply the XL-MIMO system to the HSR scenario, using near-field channel modeling as described above. We compare this with the far-field channel model commonly used in conventional MIMO systems to analyze the impact of ICI on system performance. The results show that, under near-field conditions, the SE experiences significantly less degradation as the speed increases compared to the far-field model. Therefore, near-field modeling provides a more accurate representation of system performance in XL-MIMO HSR communication, minimizing ICI effects. Moreover, while MMSE precoding outperforms MRT precoding in terms of overall performance, the degradation caused by ICI is more pronounced with MMSE precoding.

VI. CONCLUSION

In this correspondence, we exploit an analytical framework to assess the performance of the downlink XL-MIMO-OFDM HSR communication system. We derive closed-form expressions for the effective degrees of freedom (EDoF) in UPA- and ULA-based XL-MIMO systems, revealing their respective performance characteristics. Additionally, we evaluate the coverage reliability within the XL-MIMO framework. Numerical results confirm the accuracy of our findings and highlight the influence of train speed and coverage radius on signal transmission quality. Notably, increasing the number of antennas significantly improved coverage reliability. These insights are crucial for designing future HSR wireless networks. In future work, we aim to integrate the channel estimation algorithm proposed in [21] with the XL-MIMO-OFDM HSR communication system. Additionally, the estimation and compensation of DFO are crucial challenges in high-speed mobile communication. We plan to thoroughly research these issues within the XL-MIMO system, building upon previous important works [22], [23], [24]. Furthermore, we intend to compare the multiplexing gain and error performance of the XL-MIMO-OFDM system with that of the conventional MIMO-OFDM system.

REFERENCES

[1] B. Ai, A. F. Molisch, M. Rupp, and Z. -D. Zhong, "5G key technologies for smart railways," *Proc. IEEE*, vol. 108, no. 6, pp. 856–893, Jun. 2020.
[2] J. Zhang, E. Björnson, M. Matthaiou, D. W. K. Ng, H. Yang, and D. J. Love, "Prospective multiple antenna technologies for beyond 5G," *IEEE J. Sel. Areas Commun.*, vol. 38, no. 8, pp. 1637–1660, Aug. 2020.
[3] 3rd Generation Partnership Project (3GPP), "Study on performance enhancements for high speed scenario in LTE," 3GPP, Sophia Antipolis, France, Tech. Rep. 36.878, V13.0.0, Jan. 2016.
[4] Y. Ge, Q. Deng, D. G. G., Y. L. Guan, and Z. Ding, "OTFS signaling for SCMA with coordinated multi-point vehicle communications," *IEEE Trans. Veh. Tech.*, vol. 72, no. 7, pp. 9044–9057, Jul. 2023.
[5] W. Xu, Z. Yang, D. W. K. Ng, M. Levorato, and M. Debbah, "Edge learning for B5G networks with distributed signal processing: Semantic communication, edge computing, and wireless sensing," *IEEE J. Sel. Topics Signal Process.*, vol. 17, no. 1, pp. 9–39, Jan. 2023.
[6] Y. Ge, Q. Deng, P. C. Ching, and Z. Ding, "OTFS signaling for uplink NOMA of heterogeneous mobility users," *IEEE Trans. Commun.*, vol. 69, no. 5, pp. 3147–3161, May 2021.
[7] X. Zhang et al., "Cell edge user capacity-coverage reliability tradeoff for 5G-R systems with overlapped linear coverage," *IEEE Trans. Intell. Transp. Syst.*, vol. 23, no. 10, pp. 17936–17951, Oct. 2022.
[8] S. -H. Lin, Y. Xu, and J. -Y. Wang, "Coverage analysis for cell-free massive MIMO high-speed railway communication systems," *IEEE Trans. Veh. Technol.*, vol. 71, no. 10, pp. 10499–10511, Oct. 2022.
[9] J. Zheng, J. Zhang, E. Björnson, Z. Li, and B. Ai, "Cell-free massive MIMO-OFDM for high-speed train communications," *IEEE J. Sel. Areas Commun.*, vol. 40, no. 10, pp. 2823–2839, Oct. 2022.
[10] E. Björnson et al., "Towards 6G MIMO: Massive spatial multiplexing, dense arrays, and interplay between electromagnetics and processing," 2024, *arXiv:2401.02844*.
[11] Z. Wang et al., "A tutorial on extremely large-scale MIMO for 6G: Fundamentals, signal processing, and applications," *IEEE Commun. Surveys Tuts.*, vol. 26, no. 3, pp. 1560–1605, thirdquarter 2024.
[12] J. G. Proakis and M. Salehi, *Digital Communications*, New York, NY, USA: McGraw-hill, 2008.
[13] L. Wei et al., "Multi-user holographic MIMO surfaces: Channel modeling and spectral efficiency analysis," *IEEE J. Sel. Topics Signal Process.*, vol. 16, no. 5, pp. 1112–1124, Aug. 2022.
[14] J. Xu, X. Mu, and Y. Liu, "Exploiting STAR-RISs in near-field communications," *IEEE Trans. Wireless Commun.*, vol. 23, no. 3, pp. 2181–2196, Mar. 2024.
[15] Y. Liu, C. Ouyang, Z. Wang, J. Xu, X. Mu, and A. L. Swindlehurst, "Near-field communications: A comprehensive survey," *IEEE Commun. Surv. Tutorials*, 2025.
[16] Z. Wang et al., "Analytical framework for effective degrees of freedom in near-field XL-MIMO," *IEEE Trans. Wireless Commun.*, early access, Jan. 29, 2025, doi: 10.1109/TWC.2025.3531418.
[17] Y. Liu, J. Xu, Z. Wang, X. Mu, and L. Hanzo, "Near-field communications: What will be different?" 2023, *arXiv:2303.04003*.
[18] W. Jiang and H. D. Schotten, "Cell-free massive MIMO-OFDM transmission over frequency-selective fading channels," *IEEE Commun. Lett.*, vol. 25, no. 8, pp. 2718–2722, Aug. 2021.
[19] M. Mikami, K. Serizawa, Y. Ishida, H. Nishiyori, K. Moto, and H. Yoshino, "Field experimental evaluation on latency and reliability performance of 5G NR V2V direct communication in real express highway environment," in *Proc. IEEE 91st Veh. Technol. Conf.*, Antwerp, Belgium, 2020, pp. 1–5.
[20] X. Li and B. Shang, "An analytical model for coordinated multi-satellite joint transmission system," in *Proc. Int. Conf. Ubiquitous Commun.*, Jul. 2024, pp. 169–173.
[21] C. Huang, J. Xu, W. Xu, X. You, C. Yuen, and Y. Chen, "Low-complexity channel estimation for extremely large-scale MIMO in near field," *IEEE Wireless Commun. Lett.*, vol. 13, no. 3, pp. 671–675, Mar. 2024.
[22] D. Fan, Z. Zhong, G. Wang, and F. Gao, "Doppler shift estimation for high-speed railway wireless communication systems with large-scale linear antennas," in *Proc. Int. Workshop High Mobility Wireless Commun.*, 2015, pp. 96–100.
[23] T. Kim, K. Ko, I. Hwang, D. Hong, S. Choi, and H. Wang, "RSRP-based Doppler shift estimator using machine learning in high-speed train systems," *IEEE Trans. Veh. Technol.*, vol. 70, no. 1, pp. 371–380, Jan. 2021.
[24] R. Zeng, H. Huang, L. Yang, and Z. Zhang, "Joint estimation of frequency offset and Doppler shift in high mobility environments based on orthogonal angle domain subspace projection," *IEEE Trans. Veh. Technol.*, vol. 67, no. 3, pp. 2254–2266, Mar. 2018.